NEURAL TISSUE RESPONSE TO IMPACT – NUMERICAL STUDY OF WAVE PROPAGATION AT LEVEL OF NEURAL CELLS

Jiří Hozman[*], *Josef Bradáč*[†], *Jan Kovanda*[‡]

Abstract: In this article, we deal with a numerical solution of the issue concerning one-dimensional longitudinal mechanical wave propagation in linear elastic neural weakly heterogeneous media. The crucial idea is based on the discretization of the wave equation with the aid of a combination of the discontinuous Galerkin method for the space semi-discretization and the Crank-Nicolson scheme for the time discretization. The linearity of the second-order hyperbolic problem leads to a solution of a sequence of linear algebraic systems at each time level. The numerical experiments performed for the single traveling wave and Gauss initial impact demonstrate the high-resolution properties of the presented numerical scheme. Moreover, a well-known linear stress-strain relationship enables us to analyze a high-frequency regime for the initial excitation impact with respect to strain-frequency dependency.

Key words: *Wave propagation in neural medium; discontinuous Galerkin method, Crank-Nicolson scheme, high-resolution semi-implicit scheme, traveling wave, energy invariant, Gauss pulse, critical frequency*

Received: December 23, 2013 **DOI:** 10.14311/NNW.2014.24.010
Revised and accepted: April 10, 2014

1. Introduction

During its life the human organism is influenced by many different types of forces. Apart from gravitation there is a considerable amount of various forces, which have an effect on the interaction of a human body with the surrounding environment.

[*]Jiří Hozman, Technical University of Liberec, Faculty of Science, Humanities and Education, Department of Mathematics and Didactics of Mathematics, Studentská 2, 461 17 Liberec, Czech Republic, E-mail: jiri.hozman@tul.cz

[†]Josef Bradáč, ŠKODA AUTO University, Department of Automotive Technology, Na Karmeli 1457, 293 01 Mladá Boleslav, Czech Republic, E-mail: josef.bradac@savs.cz

[‡]Jan Kovanda, Czech Technical University in Prague, Faculty of Transportation Sciences, Department of Security Technologies and Engineering, Konviktská 20, 110 00, Prague, Czech Republic, E-mail: kovanda@fd.cvut.cz

As a result, activity of these forces can cause an injury of the human body under certain conditions. The scientific field which deals with a description of activities relating to the consequences of mechanical loading on the human organism is called biomechanics. The special discipline of biomechanics which is concerned with injury caused by mechanical interaction is denoted as biomechanics of injuries or trauma-biomechanics [26]. The field of trauma-biomechanics today is mostly focused on injuries sustained in traffic accidents. If we consider the world statistics, it is obvious that the highest percentage of fatal injuries falls to traffic accidents.

Among the most serious injuries during traffic accidents belong head injuries. The head injuries relating to scull and brain damage can result in a death or a permanent disability [9]. Nowadays, brain damage means significant issue, not only for its increasing volume, but mainly for its medical and economical importance. In regards to these facts, we can see the effort to decrease these serious consequences, which appear in relation with head injury. Understanding the mechanisms of head injuries is a very important condition for reducing the number of fatal consequences during traffic accidents. The knowledge obtained can be used for designing vehicle restraint systems.

1.1 Brain injury mechanisms

The brain may be the organ most critical to protect from trauma, because anatomic injuries to its structures are currently non-reversible, and consequences of injury can be devastating [22]. The wave propagation in the brain may lead to a pressure gradient with positive pressure at the site of impact and negative pressure on the opposite side of impact. Described mechanism is connected with creating intercranial compression, which causes focal injuries of the brain tissue. Consequently, the pressure gradient can give rise to shear strains within the deep structures of the brain. However, it is not yet fully understood whether the injury is due to negative pressure (tensile loading) or due to a cavitation phenomenon [4].

To be able to predict complex brain damage with a high accuracy it is important to know the reaction of brain tissue to all possibilities of mechanical loading. The development of sophisticated mathematical models of the head makes it possible to describe the brain tissue reaction during mechanical loading. The main aim of the computations is to determine the measures of prediction of the head mechanical response to impact. When combined with results of a detailed investigation of the response of the human head, such models promise to contribute substantially to the present understanding of head injury mechanisms and the impact tolerance of the head.

The subject of our interest is the mathematical model and its numerical study describing the wave propagation excited by impact at the level of neural cells together with certain possible resulting consequences to neural tissue. Let us note that the wave under consideration has a mechanical disposition, its origin is related to an initial outer energy input and it propagates in neural tissue as a shock wave, which represents one of the injury mechanisms.

1.2 Neuron-neuron interface

The neural tissue is composed of one hundred billion neurons on average, which are the basic structural components. A typical neuron includes a cell body with the diameter from 3 to 18 micrometers and an axon, which is a special cellular extension that arises from the cell body. Neurons are connected to each other to form neural network. The first works by Griffith [16] and [17] devoted to the comprehensive mathematical modeling of neural tissue can be traced back to the 1960s. In order to overcome the difficulties of modeling the large numbers of neurons these works are based on continuum descriptions in which space is continuous. These early concepts were later improved, we can cite e.g. [21]. At present, neural field theories have found applications in several areas such as the previously mentioned trauma and trauma injuries or EEG rhythms, short term memory, motion perception, etc. For recent studies of the dynamics of neural tissue we refer the reader to [10].

Because of conversion, the numerical problem of wave propagation is presented on the basic one-dimensional model which includes one neuron-neuron interface, as illustrated in Fig. 1 (top). For simplicity, the translation properties of neuron-neuron interface are modeled by a simple non-constant positive function $c(x)$ representing the so-called speed of wave propagation in the given medium, see Fig. 1 (bottom).

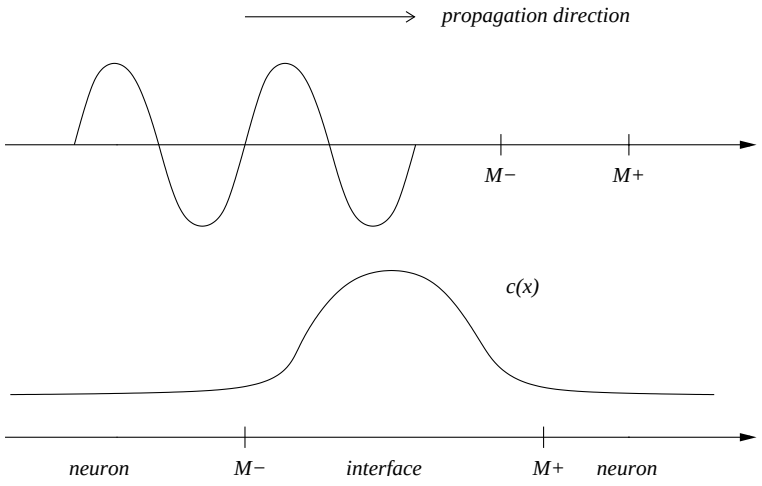

Fig. 1 *The simplified profile of propagated wave (top) and translation properties of a simplified neural medium (bottom).*

The presented numerical model considers only the mechanical concept of wave propagation in a simplified neural medium and does not describe the neuronal impulsing definitely. More precisely, our numerical study does not take into account an autonomous activity of the neural system together with an evaluation of its functional changes in the case of a damage.

2. Numerical study

The numerical schemes for solutions of the whole class of wave equations have been analyzed by many authors and several numerical studies have been introduced in the literature: from finite difference methods [15], over collocation methods [20] to finite element (FE) approaches based on Galerkin methods, e.g., [3], [14] and [19].

In this paper, we present a semi-implicit scheme for the numerical solution of the one-dimensional wave equation based on an alternative approach to the commonly used methods. The solutions of such problems usually contain subdomains, where the steep gradients or discontinuities are presented (e.g., shock waves or contact discontinuities). To solve these problems in a sufficiently robust, efficient and accurate way, we will focus on the discontinuous Galerkin (DG) methods, especially on the space-discontinuous variant of DG method, which combines the advantages of the FE method together with a discontinuous approach, for survey see [1], [8], [13] and [25]. This method is based on piecewise polynomial, generally discontinuous, approximations. From this point of view, DG methods seem to be very promising tool for the numerical simulation and provide robust and high-order accurate approximations of the solutions resulting from hyperbolic equations. Moreover, the DG concept can be easily extended by time and *hp*-adaption techniques, which enable better resolving of special situations occurred (e.g. an interaction of waves) with respect to computational meshes as well as polynomial approximation degrees, see e.g., [2] and [27].

The numerical study in the reminder of this paper focuses on high-order schemes for longitudinal one-dimensional mechanical wave propagation of pulses and harmonic waves in linear biological media represented by cerebral neural tissue.

2.1 Wave propagation in linear elastic media

Let us consider a one-dimensional problem of wave propagation through a linear medium. For small strain deformation, the equation of motion can be written as (see [23])

$$\frac{1}{\rho}\frac{\partial \sigma}{\partial x} = \frac{\partial^2 u}{\partial t^2} \quad \text{in } Q_T, \tag{1}$$

where $u(x,t)$ is the displacement in the x-direction, ρ is the mass density, and $\sigma(x,t)$ is the normal stress in the x-direction. The symbol Q_T stands for the space-time domain $I \times (0,T)$ with medium $I = (a,b)$ and final time T. For the small strain deformation considered here, the normal strain in the x-direction, $\epsilon(x,t)$, is defined as $\epsilon = \frac{\partial u}{\partial x}$ and the linear constitutive relationship of the medium is described by the linear elastic Hooke law: $\sigma = E\epsilon$, where E is the elastic Young modulus.

Substitution of $\sigma = E\frac{\partial u}{\partial x}$ into (1) yields

$$\frac{\partial^2 u}{\partial t^2} - c^2 \frac{\partial^2 u}{\partial x^2} = 0 \quad \text{in } Q_T, \tag{2}$$

where $c = \sqrt{E/\rho}$ plays a role of the speed of wave propagation in a medium I; it is usually called the phase velocity. In order to model the behaviour of propagation of wave pulse through the single interface in the medium, e.g. a membrane between

two neurons, the phase velocity is considered as a varying function $c(x) : I \to \mathbb{R}$, see an admissible shape in Fig. 1 (bottom).

The hyperbolic equation of second order (2) has to be closed with the appropriate set of prescribed initial and boundary conditions. The initial amplitude and time velocity is given by

$$u(x,0) = \varphi(x) \quad \text{and} \quad \frac{\partial u}{\partial t}(x,0) = \psi(x), \quad x \in I, \tag{3}$$

where φ and ψ are sufficiently smooth functions.

The correctness of the whole initial-boundary problem is guaranteed by the suitable choice of the boundary conditions prescribed at both endpoints of the domain I. One option here could be the natural boundary conditions given by the homogeneous Neumann boundary conditions, i.e.

$$\frac{\partial u}{\partial x}(a,t) = \frac{\partial u}{\partial x}(b,t) = 0, \quad t \in (0,T), \tag{4}$$

which represent the free endpoints (i.e. zero strain). The boundary conditions (4) belong to the kind of reflective boundary conditions, which in fact affect the solution u in the entire domain I.

To avoid the aforementioned requirement it is possible to use a sufficiently large space domain or to introduce the concept of non-reflective boundary conditions. The form of these conditions arises from the mathematical background of the equation (2), for more details see [12], and reads as

$$\frac{\partial u}{\partial t} - c(x)\frac{\partial u}{\partial x}\bigg|_{x=a} = 0, \quad t \in (0,T), \tag{5}$$

$$\frac{\partial u}{\partial t} + c(x)\frac{\partial u}{\partial x}\bigg|_{x=b} = 0, \quad t \in (0,T). \tag{6}$$

An important feature of the continuous wave equation (2) is the conservation of the total energy

$$E(t) := \frac{1}{2}\int_{-\infty}^{\infty} \left(\frac{1}{c^2(x)} \left(\frac{\partial u}{\partial t}\right)^2 + \left(\frac{\partial u}{\partial x}\right)^2 \right) \mathrm{d}x = E(0) \quad \forall\, t \in (0,T), \tag{7}$$

which directly follows from (2) by dividing by squared phase velocity c, multiplying by $\frac{\partial u}{\partial t}$ and integrating with respect to x over the real line. Then the first obtained integral is a full derivative in time and integration by parts in the second term leads to a full spatial derivative as well. Here we assume that the initial data vanish outside the domain I, and thus the integral in (7) is convergent due to the finite phase velocity. This energy conservation property (7) plays an important role in the formulation of the discrete problem. The proposed numerical scheme should preserve the energy invariant, see Section 2.4.2.

2.2 Scaled model

Now we scale the basic wave problem given by (2), (3) and (5)–(6). The characteristic quantities are length L_*, time T_* and phase velocity C_*. The characteristic

speed of wave propagation is given by $C_* = \sqrt{E_{ref}/\rho_{ref}}$, where E_{ref} and ρ_{ref} are reference values of Young's modulus and density inside the cell of neuron, respectively. Common sense suggests choosing L_* proportional to the cell size. We introduce the non-dimensional variables

$$\hat{x} = \frac{x}{L_*}, \quad \hat{t} = \frac{t}{T_*}, \quad \hat{E} = \frac{E}{E_{ref}}, \quad \hat{\rho} = \frac{\rho}{\rho_{ref}}, \quad \hat{c} = \frac{c}{C_*}, \tag{8}$$

which imply,

$$\hat{u}(\hat{x},\hat{t}) = \frac{u(x,t)}{L_*}, \quad \hat{\varphi}(\hat{x}) = \frac{\varphi(x)}{L_*}, \quad \hat{\psi}(\hat{x}) = \frac{T_*\psi(x)}{L_*}, \tag{9}$$

and from the chain rule we get

$$\frac{\partial u}{\partial x} = \frac{\partial \hat{u}}{\partial \hat{x}}, \quad \frac{\partial u}{\partial t} = \frac{L_*}{T_*}\frac{\partial \hat{u}}{\partial \hat{t}}. \tag{10}$$

Let us note that the value of $\hat{c}$ measures the rate of heterogeneity of the medium, where $\hat{c} = 1$ represents the homogeneous medium.

Substituting the dimensionless variables into the wave equation (2) with characteristic time $T_* = L_*/C_*$ gives

$$\frac{\partial^2 \hat{u}}{\partial \hat{t}^2} - \hat{c}^2(\hat{x})\frac{\partial^2 \hat{u}}{\partial \hat{x}^2} = 0 \quad \text{in } Q_{\hat{T}}, \tag{11}$$

and initial and boundary conditions become

$$\hat{u}(\hat{x},0) = \hat{\varphi}(\hat{x}) \quad \text{and} \quad \frac{\partial \hat{u}}{\partial \hat{t}}(\hat{x},0) = \hat{\psi}(\hat{x}), \quad \hat{x} \in \hat{I} = (a/L_*, b/L_*), \tag{12}$$

$$\frac{\partial \hat{u}}{\partial \hat{t}} - \hat{c}(\hat{x})\frac{\partial \hat{u}}{\partial \hat{x}}\bigg|_{\hat{x}=a/L_*} = \frac{\partial \hat{u}}{\partial \hat{t}} + \hat{c}(\hat{x})\frac{\partial \hat{u}}{\partial \hat{x}}\bigg|_{\hat{x}=b/L_*} = 0, \quad \hat{t} \in (0,\hat{T}). \tag{13}$$

In what follows we shall consider the dimensionless initial-boundary value problem given by (11)–(13) and if there is no misunderstanding the symbol $\hat{\cdot}$ will be omitted.

2.3 Transformation into conservation form

Next we rewrite the wave equation (11) as a first-order system, which is more suitable for numerical treatment. There are several algorithms to obtain a hyperbolic first-order system. However, we employ an algorithm that also guarantees the symmetry of the system, cf. [18]. Indeed, by setting the state vector

$$\boldsymbol{w}(x,t) = \begin{pmatrix} w_1(x,t) \\ w_2(x,t) \\ w_3(x,t) \end{pmatrix} = \begin{pmatrix} u(x,t) \\ \frac{\partial u}{\partial t}(x,t) \\ -c(x)\frac{\partial u}{\partial x}(x,t) \end{pmatrix} \tag{14}$$

we arrive at the system

$$\frac{\partial \boldsymbol{w}}{\partial t} + \boldsymbol{A}(x)\frac{\partial \boldsymbol{w}}{\partial x} + \boldsymbol{B}(x)\boldsymbol{w} = 0 \quad \text{in } Q_T, \tag{15}$$

where the matrices $\boldsymbol{A}$ and $\boldsymbol{B}$ are given in the following way:

$$\boldsymbol{A}(x) = \begin{pmatrix} 0 & 0 & 0 \\ 0 & 0 & c(x) \\ 0 & c(x) & 0 \end{pmatrix}, \quad \boldsymbol{B}(x) = \begin{pmatrix} 0 & -1 & 0 \\ 0 & 0 & -c'(x) \\ 0 & 0 & 0 \end{pmatrix}. \tag{16}$$

Let us note that the second equation in the above system (15) is just the original wave equation (11) written in new variables, the third one represents the symmetry of mixed derivatives, and the last one the transformation of variables. Additionally, the definition of the third component w_3 with negative sign in (14) is only for more suitable writing the equation (15) and matrix $\boldsymbol{A}$, respectively.

For convenience in the discretization of the problem, it is advantageous to represent the hyperbolic system of partial differential equations (15) in the conservation form, i.e.

$$\frac{\partial \boldsymbol{w}}{\partial t} + \frac{\partial \boldsymbol{f}(\boldsymbol{w})}{\partial x} + \boldsymbol{g}(\boldsymbol{w}) = 0 \quad \text{in } Q_T, \tag{17}$$

where

$$\boldsymbol{f}(\boldsymbol{w}) = \boldsymbol{A}(x)\boldsymbol{w} = \begin{pmatrix} 0 \\ c(x)w_3 \\ c(x)w_2 \end{pmatrix}, \tag{18}$$

$$\boldsymbol{g}(\boldsymbol{w}) = \left(\boldsymbol{B}(x) - \frac{\partial}{\partial x}\boldsymbol{A}(x)\right)\boldsymbol{w} = \underbrace{\begin{pmatrix} 0 & -1 & 0 \\ 0 & 0 & -2c'(x) \\ 0 & -c'(x) & 0 \end{pmatrix}}_{:=\boldsymbol{R}(x)}\boldsymbol{w} \tag{19}$$

are convection and reaction fluxes, respectively. Moreover, $\boldsymbol{A}(x)$ is in fact the Jacobi matrix of vector-valued function $\boldsymbol{f}$.

The new system (17) has to be equipped with the set of the initial and the boundary conditions corresponding with (12) and (13), respectively. Therefore, we close the system with the initial condition $\boldsymbol{w}(x,0) = \boldsymbol{w}^0(x),\ x \in I$, componentwisely written as

$$w_1(x,0) = \varphi(x), \quad w_2(x,0) = \psi(x), \quad w_3(x,0) = -c(x)\cdot\varphi'(x),\ x \in I, \tag{20}$$

and non-reflective boundary conditions

$$w_2(a,t) + w_3(a,t) = 0, \quad w_2(b,t) - w_3(b,t) = 0,\ t \in (0,T). \tag{21}$$

Finally, we append the relations between physical and dimensionless components of the state vector. Using (8)–(10) one obtains

$$w_1 = L_*\hat{w}_1, \quad w_2 = C_*\hat{w}_2, \quad w_3 = C_*\hat{w}_3. \tag{22}$$

2.4 Discretization

Let $\mathcal{T}_h$ $(h > 0)$ be a family of the partitions of the closure $\overline{I} = [a,b]$ of the domain I into N closed mutually disjoint subintervals $I_k = [x_{k-1}, x_k]$ with length $h_k = x_k - x_{k-1}$ and let the symbol $\mathcal{J}$ stand for an index set $\{1,\ldots,N\}$. Then we

call $\mathcal{T}_h = \{I_k,\, k \in \mathcal{J}\}$ a partition with spatial step $h = \max_{k\in\mathcal{J}}(h_k)$ and interval I_k an element. By $\mathcal{E}_h$ we denote the smallest possible set of all endpoints of all subintervals I_k, i.e. $\mathcal{E}_h = \{x_0 = a, x_1, \ldots, x_{N-1}, x_N = b\}$. Further, we label the set of all inner nodes by $\mathcal{E}_h^I$. Obviously, $\mathcal{E}_h = \mathcal{E}_h^I \cup \{a,\, b\}$.

We additionally assume that the following conditions are satisfied:

$$\exists\, C_q \geq 1 : h_k \leq C_q h_{k'} \quad \forall\, I_k, I_{k'} \in \mathcal{T}_h \text{ sharing a node} \tag{23}$$

$$\exists\, k_1, k_2 \in I\!N \text{ such that } x_{k_1} = M_- \text{ and } x_{k_2} = M_+ \tag{24}$$

The condition (23) in fact allows to control a level of the mesh refinement if adapted meshes are used and the relation (24) guarantees the membrane consistency, see Fig. 1 (top).

DG method allows us to work with different polynomial degrees over the elements. Therefore, we assign a positive integer p_k as a local polynomial degree to each $I_k \in \mathcal{T}_h$. Then we set the vector $\mathsf{p} = \{p_k, I_k \in \mathcal{T}_h\}$. Over the triangulation $\mathcal{T}_h$, we define the finite-dimensional space of discontinuous piecewise polynomial functions

$$S_{h\mathsf{p}} \equiv S_{h\mathsf{p}}(I, \mathcal{T}_h) = \{v; v|_{I_k} \in P_{p_k}(I_k)\ \forall\, k \in \mathcal{J}\}, \tag{25}$$

where $P_{p_k}(I_k)$ denotes the space of all polynomials of degree $\leq p_k$ on I_k, $I_k \in \mathcal{T}_h$. Consequently, the approximate solution of the problem given by (17) and (20)–(21) is sougth in the space of vector-valued functions $\boldsymbol{S}_{h\mathsf{p}} = [S_{h\mathsf{p}}]^3$.

Let us denote $v(x_k^+) = \lim_{\varepsilon\to 0+} v(x_k + \varepsilon)$ and $v(x_k^-) = \lim_{\varepsilon\to 0+} v(x_k - \varepsilon)$. Then we can define the jump and average of v at inner points $x_k \in \mathcal{E}_h^I$ of domain I by

$$[v(x_k)] = v(x_k^-) - v(x_k^+), \qquad \langle v(x_k)\rangle = \frac{1}{2}\left(v(x_k^-) + v(x_k^+)\right). \tag{26}$$

By convention, we also extend the definition of jump and mean value for endpoints of I, i.e. $[v(x_0)] = -v(x_0^+)$, $\langle v(x_0)\rangle = v(x_0^+)$, $[v(x_N)] = v(x_N^-)$ and $\langle v(x_N)\rangle = v(x_N^-)$. In case that $x_k \in \mathcal{E}_h$ are arguments of $v(x_k^-)$ or $v(x_k^+)$, we usually omit these arguments x_k^-, x_k^+ and write simply v^- and v^+, respectively.

2.4.1 Space semi-discretization

In this section, we recall the space semi-discrete DG scheme presented in [25]. First, we multiply (17) by a test function $\boldsymbol{v}_h \in \boldsymbol{S}_{h\mathsf{p}}$, integrate over an element $I_k \in \mathcal{T}_h$ and use integration by parts in the convection term $\frac{\partial}{\partial x}\boldsymbol{f}(\boldsymbol{w})$ of (17). Consequently, we employ a concept of a numerical flux $I\!H$ for the discretization of the convection flux and end up with the following DG formulation for the semi-discrete solution $\boldsymbol{w}_h(t)$, introduced in [11] as a system of ordinary differential equations, namely

$$\frac{\mathrm{d}}{\mathrm{d}t}\left(\boldsymbol{w}_h(t), \boldsymbol{v}_h\right) + \boldsymbol{b}_h(\boldsymbol{w}_h(t), \boldsymbol{v}_h) + \boldsymbol{r}_h(\boldsymbol{w}_h(t), \boldsymbol{v}_h) = 0 \quad \forall\, \boldsymbol{v}_h \in \boldsymbol{S}_{h\mathsf{p}}, \forall\, t \in (0, T), \tag{27}$$

where $(\cdot,\cdot)$ denotes the L^2-scalar product and the forms $\boldsymbol{b}_h(\cdot,\cdot)$ and $\boldsymbol{r}_h(\cdot,\cdot)$ stand for the semi-discrete variants of convection and reaction fluxes (18) and (19), i.e.

$$\boldsymbol{b}_h(\boldsymbol{w}(t), \boldsymbol{v}) = -\sum_{k\in\mathcal{J}} \int_{I_k} \boldsymbol{f}(\boldsymbol{w}) \cdot \boldsymbol{v}'\, \mathrm{d}x + \sum_{x\in\mathcal{E}_h} I\!H\left(\boldsymbol{w}^-(t),\, \boldsymbol{w}^+(t), n\right) \cdot [\boldsymbol{v}], \tag{28}$$

$$\boldsymbol{r}_h(\boldsymbol{w}(t), \boldsymbol{v}) = \sum_{k\in\mathcal{J}} \int_{I_k} \boldsymbol{g}(\boldsymbol{w}) \cdot \boldsymbol{v}\, \mathrm{d}x. \tag{29}$$

Further, the differential system (27) is equipped with the corresponding initial condition, prescribed in spirit of (20) as

$$\boldsymbol{w}_h(0) = \boldsymbol{w}_h^0, \qquad \text{where} \quad \left(\boldsymbol{w}_h^0 - \boldsymbol{w}^0, \boldsymbol{v}\right) \ \ \forall\, \boldsymbol{v} \in \boldsymbol{S}_{h\mathrm{p}}. \tag{30}$$

By $\boldsymbol{w}_h^0$ we denote an $\boldsymbol{S}_{h\mathrm{p}}$-approximation of the initial condition $\boldsymbol{w}^0$, which is defined as L^2-projection on space $\boldsymbol{S}_{h\mathrm{p}}$.

The essential item of the DG formulation of the model problem is the treatment of the convection part with the aid of a numerical flux. The numerical flux $\mathbb{H}(\boldsymbol{w}^-, \boldsymbol{w}^+, n)$ approximates the flux of the quantity $\boldsymbol{w}$ in the direction of n, where n stands for the outer unit normal, i.e., $n = -1$ (negative x-direction) or $n = 1$ (positive x-direction) in the one-dimensional case.

Let us note that the choice of a suitable numerical flux plays an important role, particularly in DG schemes. We can mention, e.g., the well-known Steger-Warming, Van Leer, Roe, Vijayasundaram numerical fluxes or the numerical fluxes based on the direct Riemann solver, [13]. In order to preserve the linearity of the semi-discrete problem with respect to the state vector, we utilize the Steger-Warming or Vijayasundaram numerical fluxes, which are equivalent to each other in case of a linear convection flux.

In order to determine the value of chosen numerical flux, we define the matrix

$$\boldsymbol{P}(n) = \boldsymbol{A}(x) \cdot n \quad \text{for} \quad |n| = 1, \tag{31}$$

with eigenvalues

$$\lambda_1(n) = 0, \quad \lambda_2(n) = -c \cdot n, \quad \lambda_3(n) = c \cdot n. \tag{32}$$

The matrix $\boldsymbol{P}(n)$ is diagonalizable with the aid of the matrices $\boldsymbol{T} = \boldsymbol{T}(n)$ and $\boldsymbol{T}^{-1} = \boldsymbol{T}^{-1}(n)$ as

$$\boldsymbol{P}(n) = \boldsymbol{T}\Lambda\boldsymbol{T}^{-1} \quad \text{for} \quad \Lambda = \mathrm{diag}(\lambda_1, \lambda_2, \lambda_3). \tag{33}$$

Easy computation leads to

$$\boldsymbol{T}(1) = \boldsymbol{T}(-1) = \begin{pmatrix} 1 & 0 & 0 \\ 0 & 1 & 1 \\ 0 & -1 & 1 \end{pmatrix}, \ \boldsymbol{T}^{-1}(1) = \boldsymbol{T}^{-1}(-1) = \begin{pmatrix} 1 & 0 & 0 \\ 0 & \frac{1}{2} & -\frac{1}{2} \\ 0 & \frac{1}{2} & \frac{1}{2} \end{pmatrix}. \tag{34}$$

Taking into account that matrix $\boldsymbol{P}(n)$ is diagonalizable, we define the positive and negative part of $\boldsymbol{P}$ by

$$\boldsymbol{P}(n)^{\pm} = \boldsymbol{T}\Lambda^{\pm}\boldsymbol{T}^{-1} \quad \text{for} \quad \Lambda^{\pm} = \mathrm{diag}(\lambda_1^{\pm}, \lambda_2^{\pm}, \lambda_3^{\pm}), \tag{35}$$

where $\lambda^+ = \max(\lambda, 0)$ and $\lambda^- = \min(\lambda, 0)$.

Then the numerical flux reads

$$H\left(\boldsymbol{w}^-, \boldsymbol{w}^+, n\right) = \begin{cases} \boldsymbol{P}^+(n)\boldsymbol{w}^- + \boldsymbol{P}^-(n)\boldsymbol{w}^+, & \text{if } n = 1, \\ \boldsymbol{P}^+(n)\boldsymbol{w}^+ + \boldsymbol{P}^-(n)\boldsymbol{w}^-, & \text{if } n = -1. \end{cases} \tag{36}$$

In addition, it is necessary to specify the meaning of $\boldsymbol{w}^+$ at $x = b$ and $\boldsymbol{w}^-$ at $x = a$ with respect to fulfillment of the considered boundary conditions. One

can easily observe that non-reflective boundary conditions (21) are equivalent to the well-known 'do-nothing' boundary condition, since $w_2(x_0^-) = -w_3(x_0^-)$ and $w_2(x_N^+) = w_3(x_N^+)$ imply

$$\boldsymbol{P}^-(-1)\boldsymbol{w}(x_0^-) = \boldsymbol{P}^-(1)\boldsymbol{w}(x_N^+) = 0. \tag{37}$$

2.4.2 Fully discrete DG scheme

In order to obtain the discrete solution, it is necessary to equip the scheme (27) with suitable solvers for the time integration. There is a wide range of approaches for the time discretization of ODE systems resulting from the space semi-discretization. In practical computations, the simplest time discretization is via an explicit scheme, e.g. forward Euler scheme and Runge-Kutta methods. Then we get conditionally stable methods applicable under a severe limitation on the time step due to a CFL-stability condition. However, their main advantage is an easy implementation.

On the other hand, in order to avoid the strong time step restriction of the explicit DG schemes, it is advantageous to use an implicit time discretization. Moreover, the bilinearity of the convection and reaction terms (28) and (29) directly implies that the implicit treatment in (27) corresponds to a system of linear algebraic equations without employing any additional linearization, cf. [11].

In order to present the high-order scheme with respect to the time coordinate, we introduce the fully discrete scheme for the time discretization with trapezoidal rule, giving the second order convergence in time. Equivalently, it is the average of forward Euler and backward Euler in time, well-known as the Crank-Nicolson method. The aforementioned scheme is practically unconditionally stable without any condition on the length of the time step and preserves the energy conservation property (7), see [5].

We now partition $[0,T]$ as $0 = t_0 < t_1 < t_2 < \ldots < t_M = T$, denoting each time step by $\tau_l \equiv t_l - t_{l-1}$ and let $\boldsymbol{w}_h^l$ stand for the approximate solution of $\boldsymbol{w}_h(t_l)$, $t_l \in [0,T]$, $l = 0,\ldots,M$ of problem (27) with (30). The values $\boldsymbol{w}_h^l$ at given time levels are computed according the following formula

$$\begin{aligned}(\boldsymbol{w}_h^l, \boldsymbol{v}_h) + \frac{\tau_l}{2}\left\{\boldsymbol{b}_h(\boldsymbol{w}_h^l, \boldsymbol{v}_h) + \boldsymbol{r}_h(\boldsymbol{w}_h^l, \boldsymbol{v}_h)\right\} &= (\boldsymbol{w}_h^{l-1}, \boldsymbol{v}_h) \\ -\frac{\tau_l}{2}\left\{\boldsymbol{b}_h(\boldsymbol{w}_h^{l-1}, \boldsymbol{v}_h) + \boldsymbol{r}_h(\boldsymbol{w}_h^{l-1}, \boldsymbol{v}_h)\right\} &\qquad \forall\, \boldsymbol{v}_h \in \boldsymbol{S}_{h\mathsf{p}},\ l = 1,\ldots,M,\end{aligned} \tag{38}$$

where $\boldsymbol{w}_h^0$ is $\boldsymbol{S}_{h\mathsf{p}}$-approximation of $\boldsymbol{w}^0(x)$ given by (30).

The discrete problem (38) is equivalent to a system of linear algebraic equations at each time instant $t_l \in [0,T]$. In what follows we shall be concerned with the matrix representation of the resulting linear algebraic problem.

2.4.3 Linear algebraic representation

We proceed in a similar manner to [11]. Let us introduce

$$B_k = \{\boldsymbol{v}_{k,j};\ \mathrm{supp}(\boldsymbol{v}_{k,j}) \subset I_k\}_{j=1}^{\mathrm{dof}_k}, \tag{39}$$

a local basis of the space of vector-valued discontinuous piecewise polynomial functions $\boldsymbol{S}_{h\mathsf{p}}$ defined with the aid of (25), i.e a set of linearly independent polynomial functions on $I_k \in \mathcal{T}_h$. The basis B_k belongs to the corresponding element

I_k and its dimension is given by $\mathrm{dof}_k = 3(p_k + 1)$, where p_k denotes the degree of polynomial approximation on element $I_k \in \mathcal{T}_h$. Further, a composition of local basis defines a global basis $\boldsymbol{S}_{h\mathsf{p}}$ by $B = \{\boldsymbol{v}_{k,j}; \boldsymbol{v}_{k,j} \in B_k\}_{k\in\mathcal{J}}$ and implies $\dim(\boldsymbol{S}_{h\mathsf{p}}) = \mathrm{dof} = \sum_{k\in\mathcal{J}} \mathrm{dof}_k$.

Then a function $\boldsymbol{w}_h^l \in \boldsymbol{S}_{h\mathsf{p}}$ can be written in the form

$$\boldsymbol{w}_h^l(x) = \sum_{k\in\mathcal{J}} \sum_{j=1}^{\mathrm{dof}_k} \xi_{k,j}^l \cdot \boldsymbol{v}_{k,j}(x), \quad x \in I, \quad l = 1, \ldots, M, \tag{40}$$

where $\xi_{k,j}^l \in \mathbb{R},\ l = 0, \ldots, M,\ j = 1, \ldots, \mathrm{dof}_k,\ k \in \mathcal{J}$. Moreover, for $\boldsymbol{w}_h^l \in \boldsymbol{S}_{h\mathsf{p}}$ we define the vector of its basis coefficients by

$$\boldsymbol{W}^l \equiv \left\{\xi_{k,j}^l\right\}_{j=1,\ldots,\mathrm{dof}_k}^{k\in\mathcal{J}} \in \mathbb{R}^{\mathrm{dof}}, \quad l = 1, \ldots, M \tag{41}$$

and obtain one-to-one mapping between (40) and (41).

Therefore, the linear algebraic problem (38) can be written in the matrix form

$$\left(\mathcal{M} + \frac{\tau_l}{2}\mathcal{B} + \frac{\tau_l}{2}\mathcal{R}\right)\boldsymbol{W}^l = \left(\mathcal{M} - \frac{\tau_l}{2}\mathcal{B} - \frac{\tau_l}{2}\mathcal{R}\right)\boldsymbol{W}^{l-1}, \quad l = 1, \ldots, M, \tag{42}$$

where $\mathcal{M}$ is a symmetric, positive definite block diagonal mass matrix. Each diagonal block of the matrix $\mathcal{M}$ corresponds to the appropriate element $I_k \in \mathcal{T}_h$ and its local mass matrix $\mathcal{M}_k$ set up only from basis $B_k, k \in \mathcal{J}$, i.e.,

$$\mathcal{M}_k = \{\mathcal{M}_k^{(i,j)}\}_{i,j=1}^{\mathrm{dof}_k}, \qquad \mathcal{M}_k^{(i,j)} \equiv \int_{I_k} \boldsymbol{v}_{k,j} \cdot \boldsymbol{v}_{k,i}\,\mathrm{d}x, \quad i,j = 1, \ldots, \mathrm{dof}_k. \tag{43}$$

The matrix $\mathcal{B}$ corresponds to the convection flux in the following sense as

$$\mathcal{B} = \{\mathcal{B}_{k,s}\}_{k,s\in\mathcal{J}},\ \mathcal{B} = \{\mathcal{B}_{(k,i),(s,j)}\}_{i=1,\ldots,\mathrm{dof}_k}^{j=1,\ldots,\mathrm{dof}_s},\ \mathcal{B}_{(k,i),(s,j)} = \boldsymbol{b}_h(\boldsymbol{v}_{s,j}, \boldsymbol{v}_{k,i}). \tag{44}$$

It is easy to observe that the matrix $\mathcal{B}$ is sparse and has a block structure, because the matrix element $\mathcal{B}_{(k,i),(s,j)}$ is non-vanishing only for $k = s$ (the common element) or $s = k \pm 1$ (the shared node for two neighbouring elements). The structure of the matrix $\mathcal{R}$ is formally similar to the convection matrix $\mathcal{B}$, i.e.,

$$\mathcal{R} = \{\mathcal{R}_{k,s}\}_{k,s\in\mathcal{J}},\ \mathcal{R} = \{\mathcal{R}_{(k,i),(s,j)}\}_{i=1,\ldots,\mathrm{dof}_k}^{j=1,\ldots,\mathrm{dof}_s},\ \mathcal{R}_{(k,i),(s,j)} = \boldsymbol{r}_h(\boldsymbol{v}_{s,j}, \boldsymbol{v}_{k,i}), \tag{45}$$

but the matrix element $\mathcal{R}_{(k,i),(s,j)}$ is vanishing for all $k \neq s$ (different elements) due to the definition of the reaction form $\boldsymbol{r}_h$ in (29).

3. Numerical experiments

The following section provides experimental insight into the behaviour of a mechanical wave propagation of initially excited pulses and harmonic waves in the considered neural medium. First, we describe the parameters of the numerical scheme, then the simple experiment with a single traveling wave will be used to validate the numerical code for the subsequent solving Gauss initial pulse and other types of initial conditions with respect to the wave frequencies.

3.1 Experiment settings

We consider the wave propagation in the dimensionless domain of the length corresponding to $12L_{ref}$, namely $I = [-4, 8]$ with the interface of the width d_M located at interval $I_M = [M_-, M_+] = [x_M - \frac{d_M}{2}, x_M + \frac{d_M}{2}] \subset I$ with the center x_M. The computational grid $\mathcal{T}_h$ satisfies the consistency condition for its partition given by (24). The basis functions from local basis B_k on each element I_k are associated with the corresponding Lagrange nodes according to the local polynomial degree p_k. These nodes form the principal lattice defined by

$$L(k) = \Bigg\{ x \in I_k : x = \sum_{j=1}^{2} \alpha_j x_{k-2+j},\ \alpha_1 + \alpha_2 = 1, \\ \alpha_j \in \left\{ 0, \frac{1}{p_k}, \ldots, \frac{p_k - 1}{p_k}, 1 \right\},\ j = 1, 2 \Bigg\}. \quad (46)$$

Then we can write the local basis function as

$$\boldsymbol{v}_{k,j,n} = \left(v_{k,j}\delta_{n1}, v_{k,j}\delta_{n2}, v_{k,j}\delta_{n3} \right), \quad v_{k,j} \in P_{p_k}(I_k), \quad v_{k,j}\left(N_k^{j'} \right) = \delta_{jj'}, \quad (47) \\ k \in \mathcal{J},\ j, j' = 1, \ldots, \mathrm{dof}_k,\ n = 1, 2, 3,$$

where $N_k^j \in L(k), j = 1, \ldots, \mathrm{dof}_k$ are Lagrange nodes of element I_k and the symbol $\delta_{jj'}$ stands for the Kronecker delta.

To model a medium with weak heterogeneity located at the interface, the scaled phase velocity $c(x)$, viewed in Fig. 2, is defined as

$$c(x) = \begin{cases} \frac{1}{2}(c_M - 1)\sin\left(\frac{2\pi}{d_M}(x - x_M) + \frac{\pi}{2} \right) + \frac{1}{2}(c_M + 1), & x \in I_M, \\ 1, & x \in I \backslash I_M \end{cases} \quad (48)$$

where the peak value c_M is a scaled phase velocity at the node x_M. Note that $c(x)$ is continuously differentiable and its derivative $c'(x)$ has support in interface I_M.

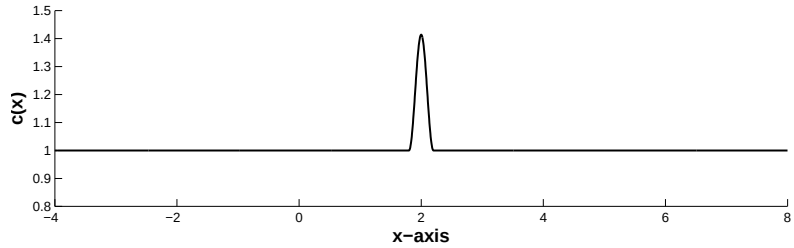

Fig. 2 *The graph of phase velocity $c(x)$ for parameters $c_M = \sqrt{2}, d_M = 0.4, x_M = 2.0$.*

Simply, it can be said about function $c(x)$ given by (48) with $c_M = \sqrt{2}$ that it represents the medium, wherein the ratio of Youngs' moduli between interface-neuron is equal to 2:1 at the same density or vice versa the ratio of densities between interface-neuron is equal to 1:2 at the same Young's modulus, respectively.

Further, to ensure sufficiently high resolution of the observed phenomena such as the wave reflection and transmission, a suitable choice of the mesh and time step has to be specified. The spatial step h has to be chosen appropriately to the wavelength and also the length of the time step τ_l does not destroy the stability of the proposed numerical scheme. Therefore, we introduce the CFL-number

$$CFL = \max_l(\tau_l) \cdot \lambda_{\boldsymbol{P}}^{max} \cdot \max_{k\in\mathcal{J}} \left(\frac{1}{h_k}\right), \tag{49}$$

where $\lambda_{\boldsymbol{P}}^{max}$ is the maximal eigenvalue of matrix $\boldsymbol{P}$ defined in (31). For explicit schemes, the stability condition reads as $CFL \leq 1$, which can be rewritten in the condition

$$\max_l(\tau_l) \cdot \max(1, c_M) \leq \min_{k\in\mathcal{J}}(h_k), \tag{50}$$

whereas the stability of the implicit scheme is guaranteed for $CFL \gg 1$ as well.

In all forthcoming numerical experiments, we set equidistant space-time discretization with steps $h = 0.005$ and $\tau = 0.001$, which in fact corresponds to the stability condition of explicit schemes up to a maximal heterogeneity rate $c_M = 5.0$ in (48). The width of the interface is $d_M = 0.4$ and its position is given by the center $x_M = 2.0$, see Fig. 2. For simplicity, we also consider a uniform polynomial approximation with the aid of piecewise linear, quadratic and cubic functions. The resulting linear algebraic problem (42) should be numerically solved at each time level $t_l \in [0, T]$. It is possible to use a direct solver which is more efficient for not too large number of degrees of freedom. For larger systems, it is suitable to use some iterative solvers. We employ the restarted GMRES solver. The restart was carried out after 50 iterations. The iterative process was stopped when the discrete l^2-norm of the residuum was smaller than 10^{-5}. The numerical computations indicate that this choice is sufficient, i.e., smaller value of the tolerance does not cause any increase of accuracy and stability of the method.

Finally, let us mention that all data used in the presented experiments are merely illustrative and can not be used for any clinical conclusions.

3.2 Traveling wave in homogeneous medium

The first example is devoted to the verification of the presented numerical scheme on the single traveling wave in homogeneous medium, i.e. we set $c_M = 1$ in (48). Let us consider the analytical single harmonic wave solution of (11) expressed as

$$u(x,t) = \frac{1}{2}\Big(1 - \cos\left(2\pi(x-t)\right)\Big) \cdot \chi_{[-1+t,t]} \tag{51}$$

where $\chi_{[-1+t,t]}$ denotes the characteristic function of the support interval $[-1+t, t]$. This exact solution represents a single wave of unit wavelength and amplitude, traveling with the unit scaled velocity in positive x-direction and located initially at the point $x_T = -\frac{1}{2}$. The initial conditions are extracted from the exact solution (51) and homogeneous Dirichlet boundary conditions correspond with non-reflective approach introduced in (13).

Fig. 3 captures the development of approximate solutions obtained by the numerical scheme (38) with piecewise linear approximation from the initial condition

to the different time instants in comparison with the exact ones given by (51). We see that the plotted approximation and the exact solutions are quite comparable, i.e. the approximate solution preserves its shape and support.

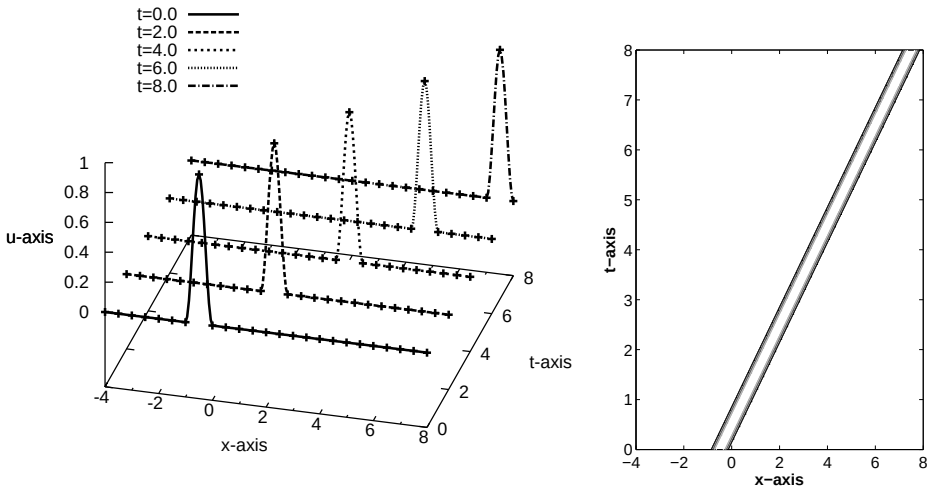

Fig. 3 *Single traveling wave: Comparison of approximate (+) and exact (−−) solutions of the single solitary wave (left) and corresponding isolines in the space-time domain (right).*

In order to illustrate the accuracy and resolution capabilities of the proposed numerical scheme, we append Tab. I monitoring the energy invariant given by (7) together with a wave amplitude. Both quantities are kept almost constant during the computation and correspond to the analytical values.

method	time t	amplitude	energy $E(t)$
present	0.0	1.0000	4.933991
method	2.0	1.0016	4.933104
	4.0	1.0032	4.932248
	6.0	1.0047	4.931405
	8.0	1.0063	4.930610
analytical val. ($c = 1.0$)	–	1.0	4.9348022

Tab. I *Single traveling wave: Computed invariant energy and amplitude.*

3.3 Gauss pulse in weakly heterogeneous medium

In the second example, we investigate the behaviour of the wave propagation through weakly heterogeneous medium with peak value $c_M = \sqrt{2}$ (see Fig. 2) after the initial impact with certain intensity and locality. Therefore, the governing equation (11) is solved under the initial zero amplitude and the initial excitation of velocity by Gauss pulse, i.e.

$$u(x,0) = 0, \quad x \in I, \tag{52}$$

$$\frac{\partial u}{\partial t}(x,0) = i_G \exp(-s_G(x-x_G)^2), \quad x \in I, \tag{53}$$

where the parameter $i_G > 0$ stands for the intensity of impact, x_G represents the center of pulse and $s_G > 0$ determine its locality. For numerical experiments, it was chosen $i_G = 1.0$, $x_G = 0.0$ and $s_G = 10$, see Fig. 4 (top left). The run of the algorithm is carried up to the time $T = 7.0$ with piecewise cubic approximation.

The set of snapshots in Fig. 4 shows the development of the approximate solutions (amplitude, velocity and strain), from the zero state into two opposite traveling waves with amplitude, which is given by the initial Gauss pulse and it is proportional to the value of the peak of this pulse and the length of its support. During the whole simulation one can easily observe the non-reflecting behaviour of traveling waves at both the endpoints of the domain and also the transmission and reflection of a wave through the interface. The exact behavior of the reflection and transmission waves depends on the phase velocity properties on both sides of the interface.

The first transition is located at $M_- = 1.8$, where the waves cross from the low speed region to the high speed one and they are partially transmitted with higher magnitude and partially reflected with unchanged polarities. On the contrary, the second transition located at $M_+ = 2.2$ corresponds to the crossing from the high speed region to the low speed one, where propagated waves are reflected with the opposite polarity and partially transmitted with lower magnitude and no phase change. This wave phenomenon is most evident in temporal velocity of the wave (see the 2^{nd} graphs in Fig. 4).

Furthermore, it is a well-known fact that the solution of the wave equation excited by a Gauss pulse contains all the possible frequencies of corresponding normal modes, because the general solution of the linear wave equation can be written as a superposition of complex-valued plane waves in the following form

$$u(x,t) = \sum_{k=1}^{\infty} A_k u_k(x,t), \quad u_k(x,t) = e^{i\phi_0} e^{ik\pi(x-ct)}, \tag{54}$$

where the positive constant A_k is an amplitude of the mode function u_k, $\phi_0 \in [0, 2\pi)$ is the initial phase, and quantity $k\pi$ is called a wave number and $\omega = ck\pi$ an angular frequency, respectively. Note that $\frac{k}{2}$ is the number of waves per unit length, i.e. a spatial frequency, while $\frac{\omega}{2}$ is the number of waves per unit time, i.e. a temporal frequency. From this point of view, it is interesting to solve the same numerical experiment with respect to the excitation frequencies, which correspond to the wavelength proportionally to the width of interface, i.e. a high-frequency regime.

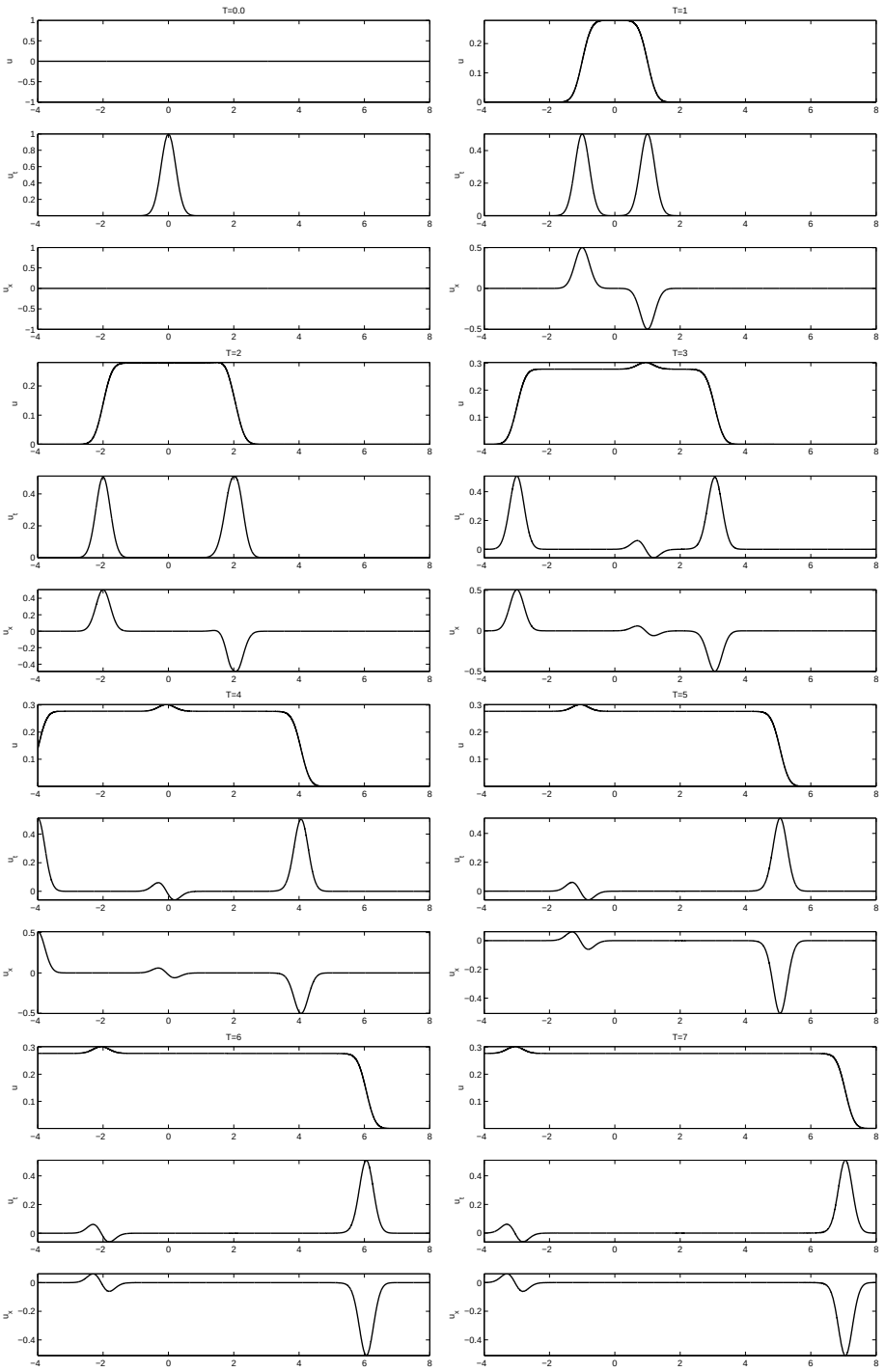

Fig. 4 *Gauss pulse: Development of dimensionless approximate solutions, u – amplitude of wave (1^{st} graph), u_t – velocity of wave (2^{nd} graph), u_x – strain (3^{rd} graph).*

3.4 Analysis of high-frequency regime

The last example analyses the influence of the excitation frequency in the initial velocity (i.e. the initial hit) on the significant (extremal) values of the strain for the fixed prescribed energy supplied to the system by the initial impact. We consider formally the same experiment setting as in the previous example of Gauss pulse, but for the several initial velocities given by

$$\frac{\partial u}{\partial t}(x,0) = \begin{cases} A_k + A_k \cos(k\pi \cdot x), & -\frac{1}{k} \leq x \leq \frac{1}{k}, \\ 0, & \text{otherwise} \end{cases}, \tag{55}$$

where A_k is the amplitude corresponding to the wave number $k\pi$. Since the initial impact is located in the region with homogeneous medium (i.e. interior of a neuron), the value of the phase velocity $c(x) \equiv 1$. Moreover, the following relation for wave number $k\pi = 2\pi f/c$ enables us to rewrite the initial condition (55) with respect to the temporal frequency f as

$$\frac{\partial u}{\partial t}(x,0) = \begin{cases} A_f + A_f \cos(2\pi f \cdot x), & -\frac{1}{2f} \leq x \leq \frac{1}{2f}, \\ 0, & \text{otherwise} \end{cases}, \tag{56}$$

where A_f is the amplitude corresponding to the frequency f. The amplitude A_f is chosen in order to guarantee the same energy of the initial wave for all considered frequencies. From (7) and (56) we obtain for the initial energy the relation

$$E(0) = \frac{1}{2}\int_{-\infty}^{\infty} \left(\frac{\partial u}{\partial t}(x,0)\right)^2 \mathrm{d}x = \frac{A_f^2}{2}\int_{-\frac{1}{2f}}^{\frac{1}{2f}} \Big(1+1\cos(2\pi f \cdot x)\Big)^2 \mathrm{d}x := E_f(0). \tag{57}$$

Therefore, we choose the amplitude A_f as a multiple of $1/\sqrt{E_f(0)}$ to obtain the corresponding square multiples of unit initial energy of the wave. We carried out the computations with the presented numerical scheme (38) with the piecewise cubic approximation over the time domain $[0, 8]$ for several initial frequencies and energies. A similar development of the approximate solutions such as amplitude, velocity and strain is observed as in Section 3.3.

Tab. II records the obtained results and illustrates the dependency between the strain and the initial excitation frequency and energy, respectively. Due to the character of the propagated wave, the significant values of strain are proportionally measured only by the maximal value of quantity $(-c\epsilon)^+$ over all the time levels t_l, i.e. the minimal value of $(-c\epsilon)^-$ does not play an important role in crossing the interface as illustrated in Fig. 4 (3^{rd} graph). Let us note that the quantity $c\epsilon$ reflects the character of the propagated wave more closely, because it also takes the properties of the medium into account. Fig. 5 depicts the development of $(-c\epsilon)^+$ at each time level with the maximal value highlighted, which corresponds with the results from Tab. II.

One can easily observe from Tab. II that the higher values of $\max_{t_l}(-c\epsilon)^+$ (i.e. extremal values of strain ϵ) are proportional to the increasing initial frequency f as well as to the increasing initial energy $E_f(0)$ of the impact. Since we consider the stress $\sigma = \sigma(\epsilon)$ as a linear function of strain ϵ, we are easily able to determine the so-called critical initial excitation frequency for fixed wave energy for each prescribed stress, for which the wave causes the significant strain resulting in an irreversible change in the medium, i.e. the corruption of neural tissue.

		$f = 1.0$	$f = 2.0$	$f = 3.0$	$f = 4.0$	$f = 5.0$
$E_f = 1.0$	$\max_{t_l}(-c\epsilon)^+$	1.5501	2.0680	2.4545	2.7829	3.0721
$E_f = 2.0$	$\max_{t_l}(-c\epsilon)^+$	2.1922	2.9246	3.4712	3.9356	4.3447
$E_f = 3.0$	$\max_{t_l}(-c\epsilon)^+$	2.6848	3.5819	4.2513	4.8200	5.3211
$E_f = 4.0$	$\max_{t_l}(-c\epsilon)^+$	3.1002	4.1360	4.9090	5.5657	6.1443

Tab. II *Strain-frequency dependency for fixed initial energy*

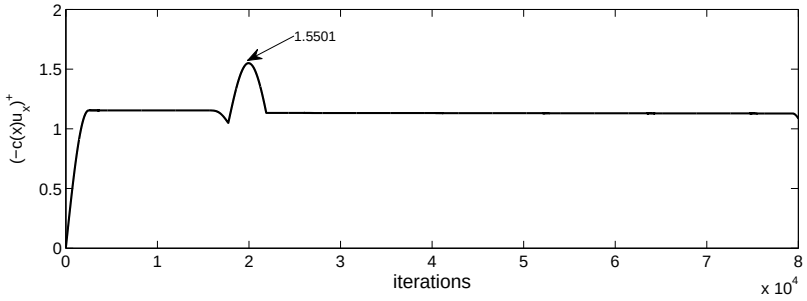

Fig. 5 *High-frequency regime: Development of quantity* $(-c(x)\epsilon)^+$ *during the whole simulation for the unit initial energy and frequency* ($E_f(0) = 1.0$ *and* $f = 1.0$).

4. Results and discussion

This paper aims to provide to the readers a deeper insight into the one of the possible computational models to deal with neural tissue injuries caused by propagating mechanical shock wave at the level of neural cells. The numerical models of these systems usually describe the tissue as a fixed set of interconnected neural cells comprised of a large amount of units with similar properties, which in fact represent the homogeneous neural medium. In contrast, our study is focused only on one neuron-neuron interface modeled by the sufficiently smooth phase velocity function supplying to the medium a certain rate of inhomogeneity. From the recent reviews devoted to the inhomogeneous neural network let us mention, e.g. [6], [7] and [24].

The introduced numerical model also has its limitations consisting in the simplification of the structure of tissue as a linear elastic medium, and in uncertain material data; namely the precise determination of Young's modulus of neuron or the compact neural tissue still remains an open problem.

On the other hand, the presented numerical experiments (Sections 3.3 and 3.4) have shown even a weak heterogeneity can dramatically influence the wave propagation in an excitable neural medium. We showed that for several amplitudes and wavelengths the main effect of the inhomogeneity located at the interface of two neurons is to reflect and transfer the original excited pulse with new changed characteristics. Moreover, if we assume sufficiently accurate input data, we shall

be able to compute stresses, which indicate the possible damage of the neural tissue, and even determine the critical frequencies inducing irreversible changes in the neural tissue.

These results give us quite good a starting point to relate the results from our model to real experiments, which would be of interest in the further study together with important extension of our current work to the two-dimensional waves. Another extension of our model can also be carried out in the sense of nonlinear medium, which is obviously more realistic from the viewpoint of neural tissue modeling.

5. Conclusion

The original problem is to describe the mechanism of a viscous injury by the pressure wave at the histological level, i.e. to find answers to what is happening with each structural component of a neuron, especially with axons and their synapses, when the wave excited by an impactive force propagates in the continuum. The above considered problem is modeled by using a simplified approach for a longitudinal one-dimensional mechanical wave propagation in linear elastic inhomogeneous media having two segments with different mechanical properties. From the mathematical point of view the linear hyperbolic wave equation of the second order describing the simplified model problem is transformed into the conservation form as a first-order system and the concept of non-reflective boundary conditions is employed. The referred special choice of transformation of variables allows us to easily compute the values of strain as one component of the state vector.

The subsequent numerical study arises from the discretization of the equation with the aid of a combination of the discontinuous Galerkin method for the space semi-discretization and the Crank-Nicolson scheme for the time discretization. The set of numerical examples produces satisfactory results and illustrates the potency of the proposed numerical scheme from traveling waves in homogeneous medium over simply excited Gauss pulses in weakly heterogeneous medium to high frequency analysis with respect to the strain-frequency dependency.

For the future work, we intend to extend the introduced model to two-dimensional case with nonlinear medium and the comparison with experimental results will be also perspective.

Acknowledgements

JH would like to thank H. Říhová for her assistance with the elaboration of numerical experiments. This work was partly supported by Technology Agency of the Czech Republic, project No. TE01020020, and by SGS Project 'Modern numerical methods II' financed by TU Liberec.

References

[1] Arnold D. N., Brezzi F., Cockburn B., Marini L. D.: Unified analysis of discontinuous Galerkin methods for elliptic problems, SIAM J. Numer. Anal. **39**(5), 2002, pp. 1749–1779.

[2] Babuška I., Suri M.: The *p*- and *hp*- fem a survey, SIAM Review **36**, 1994, pp. 578–632.

[3] Bales L., Lasiecka I.: Continuous finite elements in space and time for the nonhomogeneous wave equation, Computers Math. Applic. **27**, 1994, pp. 91–102.

[4] Bangash M. Y. H., Bangash F. N., Al-Obaid Y. F., Bangash T.: Trauma - An Engineering Analysis, Springer Berlin Heidelberg, 2007.

[5] Bangerth W., Geiger M., Rannacher R.: Adaptive Galerkin finite element methods for the wave equation, Computational Methods in Applied Mathematics **10**(1), 2010, pp. 3–48.

[6] Bressloff P. C.: Traveling fronts and wave propagation failure in an inhomogeneous neural network, Physica D **155**, 2001, pp. 83–100.

[7] Bressloff P. C., Folias S. E., Kilpatrick Z. P.: Traveling pulses and wave propagation failure in an inhomogeneous neural network, SIAM J. Appl. Dyn. Syst. **7**, 2008, pp. 161–185.

[8] Cockburn B., Karniadakis G. E., Shu C.-W.: Discontinuous Galerkin Methods, Springer, Berlin, 2000.

[9] Collins J. G.: Types of injuries by selected characteristics, Vital Health Stat. **10**, 1990.

[10] Coombes S.: Neural fields, Scholarpedia, 2006.

[11] Dolejší V., Holík M., Hozman J.: Efficient solution strategy for the semi-implicit discontinuous Galerkin discretization of the Navier-Stokes equations, Journal of Computational Physics **230**(11), 2011, pp. 4176–4200.

[12] Engquist B., Majda A.: Absorbing boundary conditions for the numerical simulation of waves, Mathematics of Computation **31**, 1977, pp. 629–651.

[13] Feistauer M., Felcman J., Straškraba I.: Mathematical and Computational Methods for Compressible Flow, Oxford University Press, Oxford, 2003.

[14] French D. A, Peterson T. E.: A continuous space-time finite element method for the wave equation, Math. Comput. **65**, 1996, pp. 491–506.

[15] Godlewski E., Raviart P. A.: Numerical Approximation of Hyperbolic Systems of Conservation Laws, Applied Mathematical Sciences **118**, Springer-Verlag, New York/Berlin, 1996.

[16] Griffith J. S.: A field theory of neural nets: I: Derivation of field equations, Bulletin of Mathematical Biophysics **25**, 1963, pp. 111–120.

[17] Griffith J. S.: A field theory of neural nets: II: Properties of field equations, Bulletin of Mathematical Biophysics **27**, 1965, pp. 187–195.

[18] Hanel C., Hörmann G., Spreitzer Ch., Steinbauer R.: Wave Equations and Symmetric First-order Systems in Case of Low Regularity, Pseudo-Differential Operators, Generalized Functions and Asymptotics Operator Theory: Advances and Applications **231**, 2013, pp. 283–296.

[19] Hughes T. J. R., Hulbert G.: Space-time finite element methods for second-order hyperbolic equations, Comput. Methods Appl. Mech. Engrg. **84**, 1990, pp. 327–348.

[20] Jung J.-H., Don W. S.: Collocation Methods for Hyperbolic Partial Differential Equations with Singular Sources, Advances in Applied Mathematics and Mechanics **1**(6), pp. 769–780.

[21] Nunez P. L.: The brain wave equation: a model for the EEG, Mathematical Biosciences **21**, 1974, pp. 279–297.

[22] Melvin J. W. et al.: Accidental Injury-Biomechanics and Prediction, Springer, New York, USA, 1993.

[23] Meurer T., Qu J., Jacobs L. J.: Wave propagation in nonlinear and hysteretic mediaa numerical study, International Journal of Solids and Structures **39**, 2002, pp. 5585–5614.

[24] Osan R., Zhang J.: Effects of synaptic connectivity inhomogeneities for propagation of activity in neural tissue, BMC Neuroscience **13**(1), 2012, pp. 76–79.

[25] Rivière B.: Discontinuous Galerkin Methods for Solving Elliptic and Parabolic Equations: Theory and Implementation, Frontiers in Applied Mathematics, SIAM, Philadelphia, 2008.

[26] Schmitt U. K.: Trauma Biomechanics, Accidental Injury in Traffic and Sports, Springer, 2010.

[27] Schwab C.: *p*- and *hp*-Finite Element Methods, Clarendon Press, Oxford, 1998.